Review

Integration Data Model of the Bathymetric Monitoring System for Shallow Waterbodies Using UAV and USV Platforms †

Oktawia Lewicka [1], Mariusz Specht [2,*], Andrzej Stateczny [3], Cezary Specht [1], Gino Dardanelli [4], David Brčić [5], Bartosz Szostak [3], Armin Halicki [2], Marcin Stateczny [2] and Szymon Widźgowski [2]

[1] Department of Geodesy and Oceanography, Gdynia Maritime University, Morska 81-87, 81-225 Gdynia, Poland
[2] Marine Technology Ltd., Wiktora Roszczynialskiego 4-6, 81-521 Gdynia, Poland
[3] Department of Geodesy, Gdańsk University of Technology, Gabriela Narutowicza 11-12, 80-233 Gdańsk, Poland
[4] Department of Engineering, University of Palermo, Piazza Marina 61, 90133 Palermo, Italy
[5] Faculty of Maritime Studies, University of Rijeka, Studentska ulica 2, 51000 Rijeka, Croatia
* Correspondence: m.specht@marinetechnology.pl
† This article is an extended version of our abstract published in Proceedings of the 15th Baška GNSS Conference: Technologies, Techniques and Applications across PNT and The 2nd Workshop on Smart, Blue and Green Maritime Technologies, Baška, Croatia, 8–13 May 2022, pp. 93–95.

Abstract: Changes in the seafloor relief are particularly noticeable in shallow waterbodies (at depths up to several metres), where they are of significance for human safety and environmental protection, as well as for which the highest measurement accuracy is required. The aim of this publication is to present the integration data model of the bathymetric monitoring system for shallow waterbodies using Unmanned Aerial Vehicles (UAV) and Unmanned Surface Vehicles (USV). As part of this model, three technology components will be created: a hydroacoustic and optoelectronic data integration component proposed by Dąbrowski et al., a radiometric depth determination component based on optoelectronic data using the Support Vector Regression (SVR) method, and a coastline extraction component proposed by Xu et al. Thanks to them, it will be possible to cover the entire area with measurements in the coastal zone, in particular between the shallow waterbody coastline and the min. isobath recorded by the echo sounder (the area is lacking actual measurement data). Multisensor data fusion obtained using Global Navigation Satellite System (GNSS)/Inertial Navigation System (INS), Light Detection And Ranging (LiDAR), Real Time Kinematic (RTK), UAV, and USV will allow to meet the requirements provided for the International Hydrographic Organization (IHO) Special Order (horizontal position error ≤ 2 m ($p = 0.95$), vertical position error ≤ 0.25 m ($p = 0.95$)). To this end, bathymetric and photogrammetric measurements shall be carried out under appropriate conditions. The water transparency in the tested waterbody should be at least 2 m. Hydrographic surveys shall be performed in windless weather and the water level is 0 in the Douglas sea scale (no waves or sea currents). However, the mission with the use of an UAV should take place in appropriate meteorological conditions, i.e., no precipitation, windless weather (wind speed not exceeding 6–7 m/s), sunny day.

Keywords: data integration; bathymetric monitoring system; shallow waterbody; Unmanned Aerial Vehicle (UAV); Unmanned Surface Vehicle (USV); hydrography

1. Introduction

The beginning of the 21st century is the era of using Unmanned Surface Vehicles (USV) in hydrographic surveys. Giordano et al. [1,2] tested a newly constructed autonomous USV (MicroVEGA) equipped with an anti-collision system, a Differential Global Positioning System (DGPS) receiver, an Inertial Navigation System (INS), a Single Beam Echo Sounder (SBES), and a vision system. Based on the tests conducted in the Marina Grande harbour in Italy, it was demonstrated that the prototype was suitable for carrying out bathymetric and geomorphological measurements in coastal waters, underwater archaeological research, monitoring the processes occurring in the coastal zone, etc. Jin et al. [3] presented a method for measuring the depth of ocean waters using an USV equipped with a GNSS Real Time Kinematic (RTK) receiver, a SBES, and based on the tide information. The validation study was conducted on the Wuzhizhou Island in China. USVs were demonstrated to be suitable for carrying out bathymetric measurements in ocean waters. Liang et al. [4] presented an integrated method for bathymetric measurements of shallow waterbodies using high-resolution satellite images GeoEye-1 and an USV equipped with a GNSS RTK receiver and a SBES. The validation study was conducted on the Wuzhizhou Island in China and demonstrated a high depth measurement accuracy (22 cm (Root Mean Square (RMS))) using an USV, as well as the possibilities for use of high-resolution satellite images and USVs to carry out bathymetric measurements in large shallow waterbodies. Lubczonek et al. [5] developed a method for integrating data acquired using Unmanned Aerial Vehicles (UAV) and USVs in order to create a digital model of the shallow waterbody bottom including both the land and water parts. The validation study was conducted on the Lake Dąbie in Poland and demonstrated that the integration of the above-mentioned methods enables the generation of a bathymetric model shallow waterbody model with an accuracy of 3 cm (RMS). Nikolakopoulos et al. [6] used UAVs and USVs to map beach rocks, i.e., well-cemented sedimentary rocks consisting of gravel, mud, and sand, which form along the coastline. The study was conducted on the Syros Island in Greece and demonstrated that thanks to the Structure from Motion (SfM) technique from the UAV and the data recorded by the echo sounder and side-scan sonar from the USV, it would be possible to find and map different geomorphological forms in shallow waters. Specht et al. [7] analysed the variability of the Territorial Sea Baseline (TSB) in three representative waterbodies of the Republic of Poland (exit from a large harbour, open sea, and river-mouth). To this end, two USVs (OceanAlpha USV SL20 and Seafloor Systems HyDrone) equipped with GNSS RTK receivers and SBESs were used. Based on the obtained results, it was concluded that the lowest variability of the TSB (1.86–3 m) was noted in the waterbody located near the Vistula Śmiała River mouth, which features steep shores (at a distance of a few metres from the coastline, the depth suddenly increases to 5 m). For this reason, changes in the TSB position are slight. On the other hand, the highest variability of the TSB (5.73–8.37 m) was noted in the waterbody adjacent to the municipal beach in Gdynia. The factors contributing to the significant changes in the TSB position included the land reclamation works performed periodically in this area and the fact that the waterbody depths increased slowly as the distance between it and the coastline increased. Specht et al. [8] carried out hydrographic surveys in the National Sailing Centre (NSC) yacht port at the Gdańsk University of Physical Education and Sport (GUPES), which were aimed at defining and developing unique bathymetric and navigational charts of the harbour and the approach fairway. The surveys were conducted using an USV (Seafloor Systems HyDrone) equipped with a GNSS RTK receiver and a SBES. The small dimensions of the USV enabled the performance of bathymetric measurements in the marina and in hard-to-reach places such as berths for yachts and other manned surface vessels (y-booms), as well as in the immediate vicinity of moored vessels or the quay. Stateczny et al. [9] presented an innovative USV (HydroDron) equipped with a GNSS/INS system, an interferometric system, a MultiBeam EchoSounder (MBES), and a sonar, intended for carrying out hydrographic surveys in restricted waters, particularly in shallow waterbodies. The main advantage of the HydroDron is the ability

to carry out bathymetric measurements with minimal human intervention, thanks to the autonomous control system. Suhari et al. [10] conducted bathymetric measurements using an improved version of the Remotely Operated Vehicle (ROV) (SHUMOO) equipped with an echo sounder, a GNSS receiver, a navigation module, and a remote sensing system on Malaysian rivers. The authors indicated what should be improved in the SHUMOO vessel in the context of conducting bathymetric measurements: the hull design should be changed, the position accuracy determined by the GNSS receiver should be improved, the distance of sounding performance from the coastal station should be increased, and autonomous control should be ensured.

UAVs are also increasingly used in hydrographic surveys. Alevizos et al. [11] performed a data fusion based on RGB and multi-spectral images recorded by the UAV (DJI Phantom 4 Pro) equipped with a Complementary Metal-Oxide-Semiconductor (CMOS) and a multi-spectral camera to determine the shallow waterbody depth. The proposed method was validated on the data measured by the USV. The study demonstrated a high degree of correlation ($R^2 > 0.75$ and Lin's coefficient > 0.80) between the results of surveys carried out by the aerial drone as compared to the USV data. Moreover, the average depth measurement error of the optoelectronic method did not exceed a value of 0.5 m. Bagheri et al. [12] proposed a method using an UAV (DJI Spreading Wings S1000) equipped with a photogrammetric camera and the SfM technique for the bathymetric measurements of shallow rivers. The validation study was conducted on the Alarm River in Iran and demonstrated that the UAV + SfM method enables the generation of a river bottom model with a resolution of 1 cm and an accuracy not exceeding 0.075 m ($p = 0.95$) for a depth of up to 0.5 m. Bandini et al. [13] used an UAV (DJI Spreading Wings S900) equipped with two photogrammetric cameras and the GNSS/INS system for monitoring the water level, as well as the performance of bathymetric measurements of cenotes and lagoons. The study was conducted on the Yucatán Peninsula in Mexico and demonstrated that the water level measurement accuracy was 5–7 cm, while the depth measurement accuracy was at a level of approx. 3.8% of the measured depth. Bandini et al. [14] carried out bathymetric surveys of a small inland waterbody using an UAV (DJI Spreading Wings S900) to which a SBES was attached with a rope. The validation study was conducted on the Lake Furesø in Denmark and demonstrated that the proposed method enabled a bathymetric measurement of a waterbody (with a depth of up to 35 m) with an accuracy of approx. 2.1% of the measured depth. Moreover, the obtained results are similar to those that can be achieved using both manned and unmanned hydrographic vessels. He et al. [15] and Kim et al. [16] developed a Geospatial Regression Method (GWR) method that is aimed at determining the depth of a shallow stream (with a depth of up to 1 m) based on RGB images taken from the UAV. The validation study was conducted on the Lake Spark in China and demonstrated that the determination coefficient (R^2) and the standard deviation of the depth measurement error (Root Mean Square Error (RMSE)) amounted to 0.88 and 1.32 m after taking into account the phenomenon of water-wave refraction and 0.85 and 1.37 m after inverting the water colour, respectively. Massuel et al. [17] carried out bathymetric measurements of a small waterbody (Hoshas) in Tunisia using an UAV (DJI F550) equipped with a photogrammetric camera and compared them with the results obtained using a DGPS receiver. The digital bottom models were then generated using the SfM technique and geostatistical estimation methods such as kriging or Triangulated Irregular Network (TIN). The study demonstrated that the depth measurement accuracy was 10 times higher for UAV surveys than that for DGPS geodetic measurements. Panlilio et al. [18] carried out bathymetric measurements using an UAV (DJI Phantom 4 Pro) equipped with a RGB camera in a shallow waterbody (with a depth of up to 2 m) adjacent to the beach in Lian, the Philippines. The study demonstrated that the depth measurement accuracy oscillates around 0.06–0.064 (RMS), after taking into account the phenomenon of water-wave refraction and the corrector surface.

Currently, one of the methods of bathymetric monitoring of shallow waterbodies is the satellite image analysis. Cao et al. [19] used multispectral images taken by the

WorldView-2 satellite to determine the waterbody depth between 0 m and 20 m. The depth measurement error ranged from 1.76 m to 2.09 m (RMS) for the water depth range between 5 m and 20 m. However, in ultra-shallow depths (0–5 m), much larger errors were obtained. The method proposed by Popielarczyk et al. [20] consisted of using the integrated Global Navigation Satellite System (GNSS), Robotized Total Station (RTS), and SBES measurements, which were performed on the manned vessel. The proposed method makes it possible to determine the waterbody depth with accuracy of several centimetres. The disadvantage of this solution is the range of recorded data. It was impossible to obtain bathymetric data near the coast, so as not to damage the measurement equipment and the vessel. Another interesting solution is the possibility of determining the waterbody depth based on a publicly available database. Khazaei et al. [21] developed a novel GLObal Bathymetric (GLOBathy) database, which contains 1.4 million inland waterbodies (lakes). The GLOBathy database uses GIS tools to generate bathymetric charts based on the max depth, as well as the geometry and physical attributes of a waterbody from the HydroLakes database. Another measurement method is a bathymetric monitoring of waterbodies using unmanned platforms. Erena et al. [22] used ROV, UAV, and USV to determine the tank capacity. The aim of this article was not a bathymetric monitoring of the reservoir and the obtained depth measurement errors were not given. However, it can be judged to be fully satisfactory and to meet the accuracy requirements for the International Hydrographic Organization (IHO) Special Order. In recent years, the use of bathymetric Light Detection And Ranging (LiDAR) has been a rapidly developing method of bathymetric monitoring of waterbodies. Pratomo et al. [23] used a manned aircraft equipped with a bathymetric LiDAR for assessing the penetration capability of the green light of the Airborne LiDAR Bathymetry (ALB) in shallow water areas. The results of bathymetric measurements were referenced to GNSS RTK measurements. The depth measurement accuracy was 23.9 cm (p = 0.95). Wang et al. [24] used an UAV equipped with a lightweight bathymetric LiDAR for hydrographic surveys of shallow waterbodies and detecting underwater objects. The study demonstrated that the water table measurement accuracy was 0.123 m, while the absolute depth measurement accuracy was 0.127 m. As compared to the Airborne Laser Scanning (ALB) system, the bathymetric LiDAR obtained a higher spatial resolution (42 points/m^2), and the max depth measured by it was 1.7–1.9 of the Secchi depth. It should be remembered that the disadvantage of this solution is the high cost of purchasing/renting a bathymetric LiDAR and the appropriate water transparency in the tested waterbody.

The examples of the use of UAVs and USVs described above show how significant bathymetric shallow waterbody monitoring is [24–26]. Hence, for the purposes of the INNOvative autonomous unmanned BAThymetric monitoring system for shallow waterbodies (INNOBAT) project [27], it was decided to create an integrated system using autonomous unmanned aerial and surface vehicles, intended for bathymetric monitoring in the coastal zone. The system will enable the seabed relief to be surveyed in accordance with the requirements laid down for the IHO Special Order [28]. For the purposes of the study, autonomous unmanned measurement platforms, i.e., aerial and surface vessels that move autonomously (without human intervention) along precisely planned routes will be used. Bathymetric measurements using UAVs and USVs can be conducted up to the max depth which may be recorded by a MBES.

The bathymetric and topographic system will enable, as compared to other popular bathymetric monitoring systems, such as hydroacoustic sounding in ultra-shallow waterbodies using classical manned vehicles [29] and methods for determining waterbody depths using high-resolution satellite images [30–32], the accurate and precise measurement of the entire coastal relief. It will be possible thanks to data acquired using a GNSS receiver, a LiDAR, and a photogrammetric camera that will be installed on an UAV, as well as using a GNSS receiver and a MBES that will be mounted on an USV. LiDAR data will enable the development of a digital land model. The images taken using a photogrammetric camera will enable the determination of both the waterbody coastline course and the depth of the waterbody between the coastline and the min. isobath recorded by

an echo sounder installed on an USV. The remaining part of the seabed will be measured using an integrated hydrographic system (GNSS receiver and MBES) mounted on an USV. Further on, the image transformation methods of addition and extraction will be applied to develop the final Digital Terrain Model (DTM) of the coastal zone, which will enable an assessment of the hydrographic and navigation situation in the shallow waterbody (Figure 1) [27]. One of the most popular methods for modelling the seabed in hydrography will be used to create the DTM model, namely B-splines, Grid, Non-Uniform Rational B-Spline (NURBS) or TIN [33–35]. Based on data recorded during the measurement campaigns, the method that best approximates the seafloor will be selected.
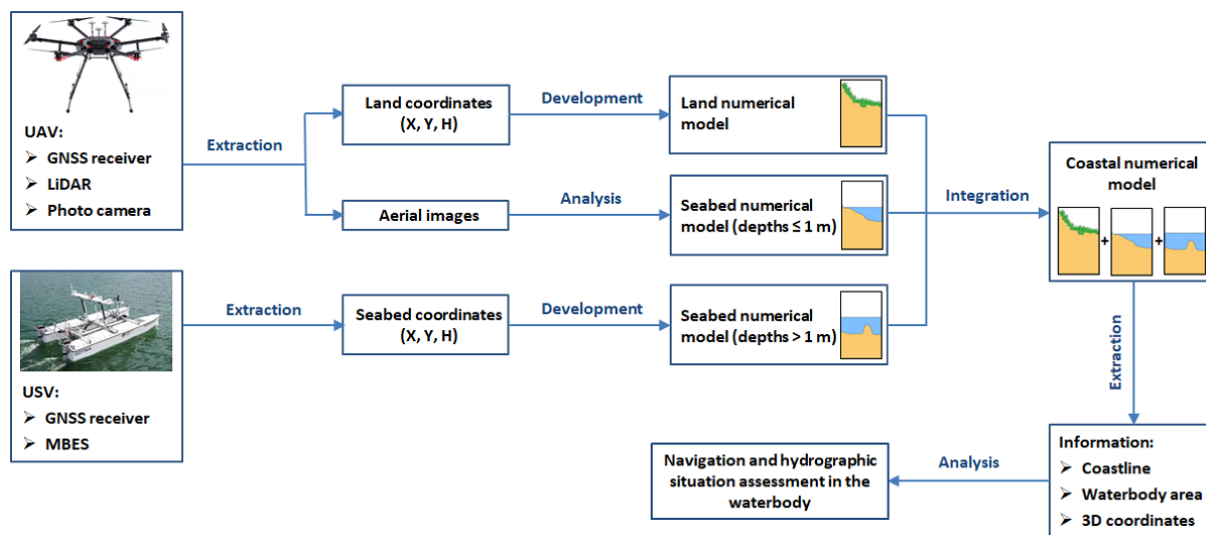

Figure 1. A diagram of the operation and functioning of an innovative autonomous unmanned system for bathymetric monitoring of shallow waterbodies [27].

The following measurement equipment will be used to test the INNOBAT system:

1. Aurelia X8 Standard UAV by the Aurelia Technologies Inc. [36];
2. Two GNSS/INS systems by the SBG Systems: Ellipse-D [37] which will be mounted on the UAV and Ekinox2-U [38] which will be placed on the USV;
3. Puck LITE LiDAR by the Velodyne Lidar [39];
4. α6500 camera [40] and E 35mm F1.8 OSS lens [41] by the Sony Corporation, as well as T3V3 camera stabiliser by the Gremsy [42];
5. HydroDron USV by the Marine Technology Ltd. [43];
6. 3DSS-DX-450 sonar by the Ping DSP Inc. [44].

In order for the INNOBAT system to operate, it is also necessary to develop the data acquired by autonomous unmanned aerial and surface vehicles, which will produce a DTM in the coastal zone. Therefore, the aim of this publication is to present the integration data model of the bathymetric monitoring system for shallow waterbodies using UAVs and USVs. As part of this model, three technology components will be created: a hydroacoustic and optoelectronic data integration component, a radiometric depth determination component based on optoelectronic data, and a coastline extraction component.

2. Materials and Methods

2.1. Hydroacoustic and Optoelectronic Data Integration Component

The first stage of work involved a review and analysis of the existing hydroacoustic and optoelectronic data integration methods. To this end, four selected data integration methods [22,45–47] were described in detail in the publication [48]. Of the many methods, those that used data derived from GNSS, RTK measurements, hydrographic surveys, a photogrammetric pass using unmanned vehicles, and Terrestrial Laser Scanning (TLS)

were selected. Moreover, the accuracy analysis of selected data integration methods had to be performed.

The assessment of the applied mathematical assumptions in data integration [45] was verified on the basis of the characteristic point coordinates of the TLS cloud related to the PL-2000 plane coordinate system, which were compared to the coordinates obtained from land GNSS measurements. The deviation values did not exceed 0.016 m in the horizontal plane, however, the deviation values did not exceed 0.027 m in the vertical plane. This proves the accuracy of the harmonisation process. No verification procedures were performed for the GNSS, TLS, UAV, and USV data integration methods [22]. In the case of data integration accuracy [46], the RMSE of the interpolated Topographic Point Cloud (TPC) amounted to 0.13 m for the northing, 0.15 m for the easting, and 0.007 m for the height coordinate. The TPC was referenced to Ground Control Points (GCP) (markers with a diameter of 0.18 m), which were determined based on GNSS RTK measurements. The accuracy of the point cloud generated by the SfM method is comparable with the data from LiDAR (accuracy at the level of 0.15–0.25 m). It is also worth paying attention to the procedure of selecting the best interpolation method for bathymetric data. The values of Mean Absolute Error (MAE), R^2, and RMSE were calculated for the interpolated Bathymetric Point Cloud (BPC) with respect to the TPC. According to the proposed accuracy assessment, the Inverse Distance Weighting (IDW) was selected. The RMSE value (0.18 m) of the interpolated BPC in relation to the TPC indicates a high degree of model fitting. The coefficient of determination also indicated a very high model fitting (0.90). On the other hand, the integration of large-scale data [47] processed into two numerical models (BPC and TPC) was characterised by high accuracy. The accuracy was assessed by comparing the bathymetric model with precise reference data. As a result, the RMSE value of 0.43 m was obtained. The description and accuracy of selected GNSS, hydroacoustic, and optoelectronic data integration methods used in hydrography are presented in Tables 1 and 2.

Table 1. A list of selected GNSS, hydroacoustic, and optoelectronic data integration methods used in hydrography.

Author and the Year of Publication	Description of the Method
Erena M. et al., 2019 [22]	The method of data integration was developed based on GNSS, TLS, UAV, and USV measurements in the Segura River Basin (Spain). The aim of the study was to present an example of the use of data fusion in monitoring quantitative changes in water resources.
Dąbrowski P.S. et al., 2021 [45]	The method of data integration was developed based on land GNSS measurements, laser scanning, and hydrographic [29] and photogrammetric [49] surveys conducted in 2019 during the tombolo phenomenon measurement campaign in Sopot (Poland). The aim of the study was to discuss the geometric aspect of geodetic harmonisation, as well as present research results based on both theoretical aspects and practical verification of the methodology.
Genchi S.A. et al., 2020 [46]	The method of data integration was developed based on UAV and USV measurements conducted in November 2018 and January 2019, respectively, in the Bahia Blanca Estuary (Argentina). The aim of the study was to present a methodological proposal to generate a topobathymetric model, using low-cost unmanned platforms in a very shallow/shallow and turbid tidal environment.
Gesch D. and Wilson R., 2001 [47]	The method of data integration was developed based on the National Oceanic and Atmospheric Administration (NOAA), United States Geological Survey (USGS), as well as LiDAR data in Tampa Bay (USA). The aim of the study was to develop techniques and tools to facilitate the integration of data derived from different sources.

Table 2. Accuracy of selected GNSS, hydroacoustic, and optoelectronic data integration methods used in hydrography [48].

Measurement Accuracy	Method According to Dąbrowski P.S. et al.	Method According to Genchi S.A. et al.	Method According to Gesch D. and Wilson R.
dN [1]	0.023 m	–	–
dE [2]	0.16 m	–	–
dNH [3]	0.027 m	–	–
RMSEx [4]	–	0.15 m	–
RMSEy [5]	–	0.18 m	–
RMSEz [6]	–	0.007 m	–
RMSE [7]	–	0.18 m	–
MAE [8]	–	0.05 m	–
R[2] [9]	–	0.90	–
RMSE [10]	–	–	0.43 m

Max difference in northing [1], easting [2], and normal height [3] coordinates with respect to reference points. RMSE of x [4], y [5], and z [6] coordinates with respect to the SfM model and 7 GCPs. RMSE [7], MAE [8], and R[2] [9] with respect to the BPC and TPC models. RMSE [10] with respect to the bathymetric grid and reference transect data.

For the purposes of the INNOBAT project applications, it was decided to choose the data integration method proposed by [45]. The reason for this choice was the highest accuracies of the geospatial data harmonisation among all of the analysed integration methods [22,45–47]. Obviously, it should be noted that the authors of the above-mentioned publications used different measurement techniques and geospatial data with different coordinate systems in their studies, as well as carried out the surveys on different waterbodies. Moreover, the authors of the method [45] were the only ones to describe in detail the mathematical procedures, which enable the creation of a 3D terrain model of the coastal zone based on the data recorded by hydroacoustic and optoelectronic devices.

The data integration method [45] was developed on the basis of the tombolo (salient) measurement campaign in Sopot in 2019, during which GNSS, TLS, UAV, and USV measurements were performed (Figure 2). In this method, the problem of indeterminacy of geodetic and hydrographic coordinate systems during the data integration process was identified. Hence, the mathematical procedures are described in detail, which allow the data to be transformed to a uniform 3D coordinate system.
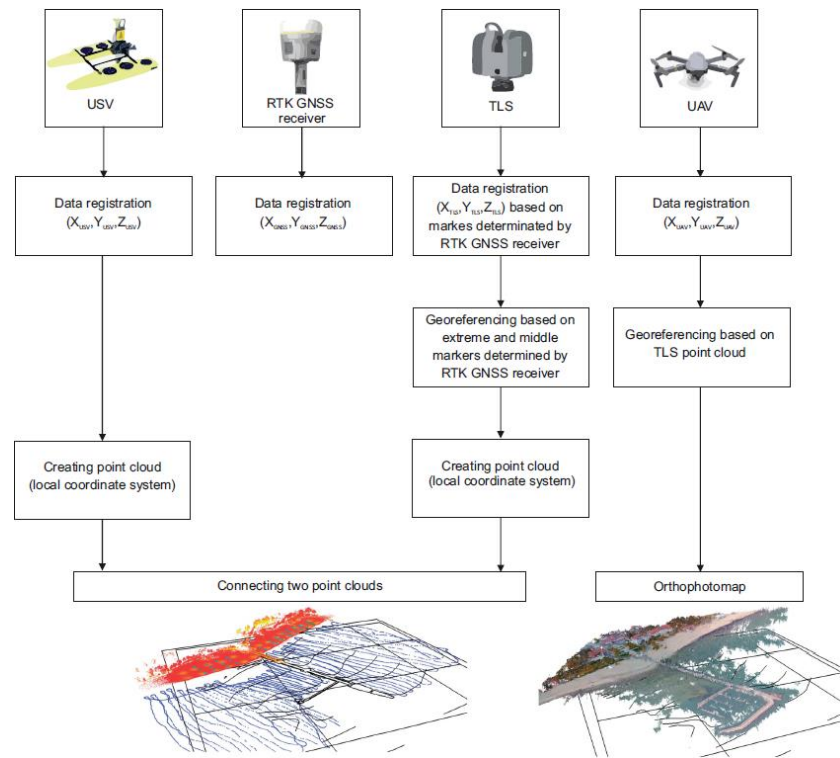
Figure 2. A simplified block diagram presenting the GNSS, TLS, UAV, and USV data integration according to [48].

Before commencing the geospatial data harmonisation, the target 3D coordinate system needs to be chosen. The authors of the method [45] adopted the plane coordinate system PL-2000 (designed for large-scale applications in Poland), while relating the normal heights to the zero ordinate of the gauging station in Kronstadt (PL-KRON86-NH).

The geospatial data harmonisation begins with determining several variables [45]:

1. Direction angles (δ) (°);
2. Averaged rotation angle (θ) (°);
3. Three elementary rotation matrices around the axes OX, OY and OZ of the 3D coordinate system (R_x, R_y, R_z) (–);
4. Scale factor (S) (–);
5. Three-dimensional coordinates of the translation vector ($\vec{T_x}, \vec{T_y}, \vec{T_z}$) (–).

After calculating the parameters: δ, θ, R_x, R_y, R_z, S, and $\vec{T_x}, \vec{T_y}, \vec{T_z}$, the point coordinates in the local based coordinate system (x^d, y^d, z^d) (m), which were recorded by hydroacoustic and optoelectronic devices, can be determined based on the formulas:

$$x^d = S \cdot R_x(\theta) \cdot x^{'} + \vec{T_x} \tag{1}$$

$$y^d = S \cdot R_y(\theta) \cdot y^{'} + \vec{T_y} \tag{2}$$

$$z^d = S \cdot R_z(\theta) \cdot z^{'} + \vec{T_z} \tag{3}$$

where:
$x^{'}, y^{'}, z^{'}$ —point coordinates in the local modified coordinate system (m).

In the data integration model presented above [45], certain modifications needed to be introduced for it to be used for the purposes of the INNOBAT system [27]. As the model will be used for bathymetric measurements of shallow waterbodies, the system PL-Universal Transverse Mercator (UTM) was adopted as the target plane coordinate system. It is created based on the mathematically unique alignment of points on the reference ellipsoid World Geodetic System 1984 (WGS-84) to the corresponding points on the plane according to the theory of transverse Mercator projection [50]. According to [51], the system PL-UTM is used for the purposes of publishing standard cartographic compilations at scales ranging from 1:10,000 to 1:250,000, nautical charts, and other maps intended for national security and defence purposes.

Another significant element is the standardisation of normal heights determined by measurement instruments. The depths and heights in Poland should be related to the vertical reference system, i.e., the so-called chart datum [52]. In marine cartography, the vertical reference system is defined as the reference level against which the sea depths and changes in the sea level are given. According to [53], the depths of waterbodies in Poland can be related to two height systems, i.e., Amsterdam (PL-EVRF2007-NH) and Kronstadt (PL-KRON86-NH). The height system PL-KRON86-NH shall be used until the implementation of the height system PL-EVRF2007-NH throughout the country, but no later than 31 December 2023.

As regards the depths measured by an echo sounder, the water level changing during hydrographic surveys needs to be taken into account. To this end, the normal height of the point measured by a hydroacoustic instrument must be calculated in the system PL-EVRF2007-NH ($H_{PL\text{-}EVRF2007\text{-}NH}$) (cm) or PL-KRON86-NH ($H_{PL\text{-}KRON86\text{-}NH}$) (cm) based on the following formulas [29]:

$$H_{PL-KRON86-NH} = -\left(d + \Delta d_E \pm \Delta d_{PL-KRON86-NH}\right) \qquad (4)$$

$$H_{PL-EVRF2007-NH} = -\left(d + \Delta d_E \pm \Delta d_{PL-EVRF2007-NH}\right) \qquad (5)$$

where:

$H_{PL\text{-}KRON86\text{-}NH}$—normal height of the point measured by echo sounder in the PL-KRON86-NH height system (cm),

$H_{PL\text{-}EVRF2007\text{-}NH}$—normal height of the point measured by echo sounder in the PL-EVRF2007-NH height system (cm),

d—depth measured by the echo sounder (cm),

Δd_E—draft of the echo sounder transducer (cm),

$\Delta d_{PL\text{-}KRON86\text{-}NH}$—depth correction referred to the chart datum in the PL-KRON86-NH height system (cm), which needs to be added where the averaged water level ($\bar{d}_{SW}$) does not exceed 508 cm, otherwise, it needs to be subtracted,

$\Delta d_{PL\text{-}EVRF2007\text{-}NH}$—depth correction referred to the chart datum in the system PL-EVRF2007-NH height system (cm), which needs to be added where the averaged water level ($\bar{d}_{SW}$) does not exceed 500 cm, otherwise, it needs to be subtracted.

However, it should be noted that the depth correction (Δd) is defined as follows [29]:

$$\Delta d_{PL-KRON86-NH} = 508\,cm - \bar{d}_{SW_{PL-KRON86-NH}} \qquad (6)$$

$$\Delta d_{PL-EVRF2007-NH} = 500\,cm - \bar{d}_{SW_{PL-EVRF2007-NH}} \qquad (7)$$

where:

$\bar{d}_{SW_{PL-KRON86-NH}}$ —averaged sea level observed on a tide gauge between consecutive full hours in the PL-KRON86-NH height system (cm),

$\bar{d}_{SW_{PL-EVRF2007-NH}}$ —averaged sea level observed on a tide gauge between consecutive full hours in the PL-EVRF2007-NH height system (cm).

The depth correction is determined by the reference system to which the zero ordinate of the gauging station is referenced. In Poland, the majority of gauging stations have an elevation of 500 cm in the system PL-EVRF2007-NH or 508 cm in the system PL-KRON86-NH. The determination of the depth correction is extremely important as water level changes can range from a few to several cm in 1 h. However, in order to ensure high measurement accuracy, hourly registration of water levels at the gauging stations might not be sufficient. Therefore, the current water level read from the gauging station should be compared to the water level calculated from the Tide Tables issued annually by the British Admiralty [54,55].

It is also important to choose the appropriate gauging station. It should be emphasised that no international legal act regulating the rules for carrying out hydrographic surveys specifies the method for acquiring water level data. However, it appears most reasonable to acquire this information from a gauging station located nearest to the site of carrying out hydrographic surveys. The method for reading the water level from a gauging station is presented in Figure 3 [56].
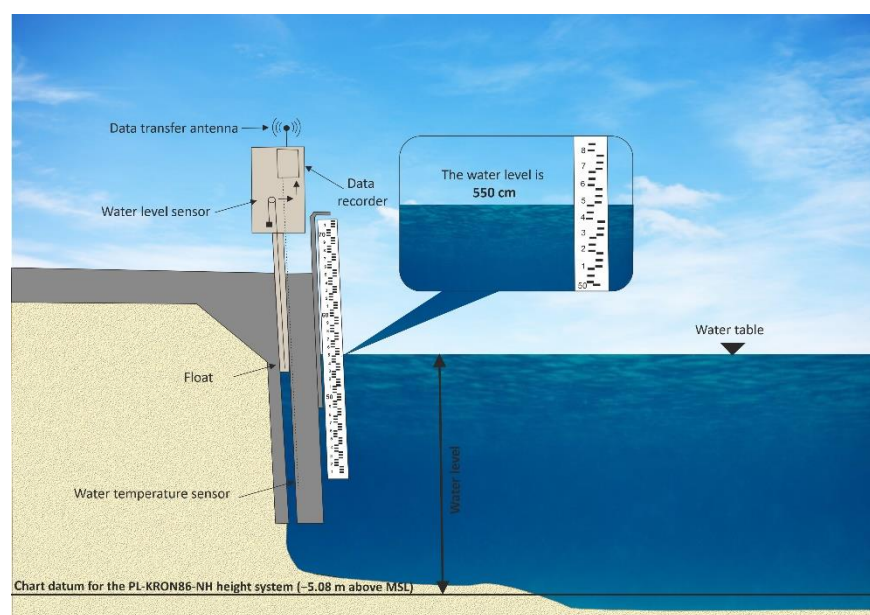

Figure 3. Diagram of a water level measurement carried out by the Institute of Meteorology and Water Management (IMGW-PIB) in Poland [56].

2.2. Radiometric Depth Determination Component Based on Optoelectronic Data

The first stage of work involved a review and analysis of six methods for determining shallow waterbody depths based on the images taken by an UAV. These algorithms included: cBathy [57], Depth Inversion [58], Support Vector Regression (SVR) [59], UAV-SfM [12], uBathy [60], and UAV-Derived Bathymetry (UDB) [61]. They were described in Table 3.

Table 3. A list of methods for determining shallow waterbody depths based on the images taken by an UAV.

Author and the Year of Publication	Description of the Method
Bagheri O. et al., 2015 [12]	The UAV-SfM method is based on the application of UAV imagery and SfM processing. To be able to validate this algorithm, photogrammetric surveys were conducted using the UAV (DJI Phantom 3 Pro) on the urban Victoria Beach located on the Alarm River (Iran).
Holman R. et al., 2013 [57]	The cBathy is based on observations of surface wave movements over long time series. The estimation of bathymetry is possible by determining the relation between the wave velocity and the depth. To be able to validate this algorithm, photogrammetric surveys were conducted using the Unmanned Aerial System (UAS) (3D Robotics X8+ platform) at two locations: on a waterbody located at the Field Research Facility (FRF) in Duck and on the Agate Beach coastline (USA).
Hashimoto K. et al., 2021 [58]	The Depth Inversion is based on wave propagation resulting from the combination of the wind force, its duration, and the gravitational force which is detected from video image. To be able to validate this algorithm, photogrammetric surveys were conducted using the UAV (DJI Phantom 4) in ocean waters located in the Suruga Bay (Japan).
Agrafiotis P. et al., 2019 [59]	The SVR is based on computation of the linear regression model in a multidimensional feature space. To be able to validate this algorithm, photogrammetric surveys were conducted using the UAV (Swinglet CAM) in Agia Napa and Amathouda (Cyprus).
Simarro G. et al., 2019 [60]	The uBathy is based on the Principal Component Analysis (PCA) of the Hilbert transform as a function of time. The process is carried out on video images in order to determine the frequency and wave number for individual wave components. To be able to validate this algorithm, photogrammetric surveys were conducted using the UAV (DJI Phantom 3 Pro) on the urban Victoria Beach located on the southwestern coast of Spain (Atlantic Ocean).
Tonion F. et al., 2020 [61]	The UDB is based on the Satellite-Derived Bathymetry (SDB) method, which uses algorithms that operate based on multi-spectral images, which are able to ensure a spectral resolution higher than RGB images by recording image data in specific electromagnetic spectrum range. To be able to validate this algorithm, photogrammetric surveys were conducted using the UAV (Spreading Wings S1000) in an area located on the Tyrrhenian Sea coast (Italy).

The main criteria for the assessment of methods for determining shallow waterbody depths included the depth measurement accuracy, hydrometeorological conditions occurring during the performance of photogrammetric surveys, and the measurement equipment used. For most algorithms (cBathy, Depth Inversion, SVR, uBathy, and UDB), the depth RMSE values were provided and summarised in Table 4. The RMSE measure was selected because it is the most commonly applied criterion to assess the accuracy of the algorithms used for depth determination. It should be concluded that the RMS measures obtained for the algorithms cBathy (0.17–0.34 m), Depth Inversion (0.33–0.52 m), SVR (0.11–0.50 m), and uBathy (0.38–0.73 m) are close to each other. Where the UDB method was applied, a high depth measurement accuracy was obtained for the range of 0–5 m (0.24–0.37 m). However, it should be noted that this accuracy decreases with an increase in the depth, as the depth measurement error range was several times greater (0.89–1.06 m). As regards the UAV-SfM method, a verification study was conducted, but another statistical measure of the depth measurement accuracy was applied. The authors of the UAV-SfM method wrote that the R95 measure was 0.075 m for clean waterbodies with a depth not exceeding 0.5 m.

Table 4. Summary of the depth RMSE values for the cBathy, Depth Inversion, SVR, uBathy, and UDB methods. Own study based on [57–61].

Method			RMSE (m)
cBathy			0.17–0.34
Depth Inversion			0.33–0.52
SVR	Depth range: 0.1–5.57 m		0.11–0.19
	Depth range: 0.2–14.8 m		0.45–0.50
uBathy	Video 1	t_f = 0 s	−
		t_f = 5 s	0.42–0.73
		t_f = 10 s	0.47–0.59
	Video 2	t_f = 0 s	0.38–0.44
		t_f = 5 s	0.38–0.46
UDB	Depth range: 0–5 m	Lyzenga	0.24
		Stumpf	0.37
	Depth range: 0–11 m	Lyzenga	0.89
		Stumpf	1.06

The cBathy, Depth Inversion, and uBathy algorithms used to determine shallow waterbody depths make use of the phenomenon of water-wave refraction that is modelled based on the acquired video images. This fact prevented the use of these algorithms as the waving is often accompanied by strong winds, which significantly hinders surveys using UAVs. Another disadvantage of the above-mentioned algorithms is the impossibility of carrying out bathymetric measurements on inland waterbodies, where virtually no wave action occurs.

The UAV-SfM is an algorithm that satisfies the design requirements, yet it was not selected as the target method for determining the depth of a shallow waterbody. This is due to the fact that it requires time-consuming and manual work to be performed in the post-processing. It is based on the SfM technique used to obtain a point cloud. The points found under the waterbody surface must then be selected and corrected because of the phenomenon of light beam refraction when the medium in which it moves changes.

The UDB algorithm requires that data be acquired using a multi-spectral camera so that mathematical operations can be performed on electromagnetic wave spectra outside the visible light spectrum. As part of the INNOBAT project, a high-resolution digital camera was purchased, but it is not able to record other wave spectra than that of visible light. Therefore, this algorithm cannot be used.

The SVR algorithm is not directly intended for solving problems concerning the determination of waterbody depths. This is an algorithm designed to perform the linearisation of a selected issue. This solves the problem of light beam refraction when the medium changes. The creation of a mathematical model enables considerable automation of the data processing. The authors of the method stress that work based on this model allows the accuracy requirements provided for the IHO Special Order to be satisfied (vertical position error ≤ 0.25 m (p = 0.95)) [28]. Another advantage of the SVR algorithm is the favourable hydrometeorological conditions (uniform illumination of the test area and windless weather) from the perspective of the photogrammetric survey performance using an USV. Furthermore, no specialised measurement equipment, i.e., a drone with a digital camera installed, is required. Therefore, it was decided to choose the method proposed by [59] to determine the shallow waterbody depths based on an analysis of images taken by UAV.

SVR [62] is an algorithm that operates based on the calculation of the linear regression function in a multi-dimensional space of features (Figure 4) [63]. The model is to enable a more accurate determination of the depth of point clouds obtained based on the SfM tech-

nique by eliminating the phenomenon of water-wave refraction [64]. SfM [65] is a technique, whose task is to provide three-dimensional scenes using a series of temporal RGB images and georeferencing information. It also provides information on the internal and external camera orientation at the time of acquiring each image by using automatic algorithms for estimating its location. This results in a model that enables the determination of how individual 3D coordinates are projected on the images from the camera [66,67]. After generating the SfM point cloud, one of the five popular vegetation filter alogrithms will be used to clean it [68]:

1. Ground point classification based on a Vegetation Index (VI);
2. TIN densification, or adaptive TIN, as implemented in LAStools (TIN) [69,70];
3. Photoscan native filtering algorithm [71];
4. Iterative Surface Lowering (ISL) [72];
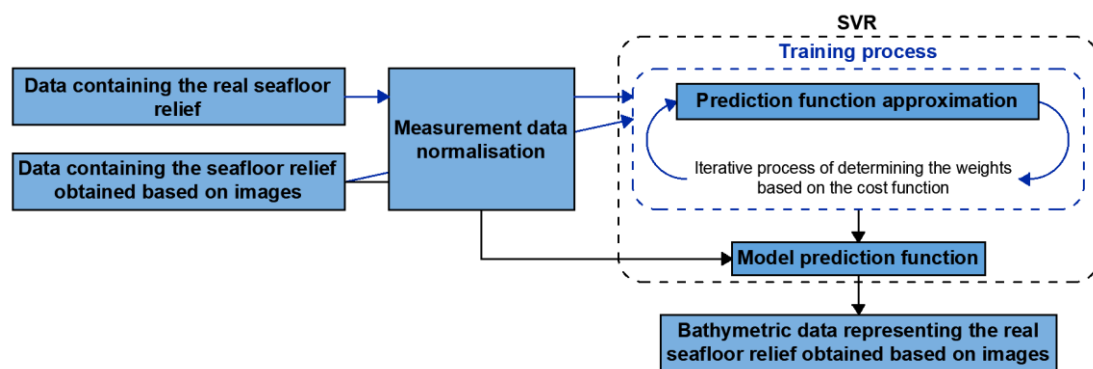5. A combination of ISL and VI (ISL_VI).

Figure 4. Diagram of the SVR algorithm's operation. Own study based on [59].

Before commencing work with the SVR algorithm, the process of input data standardisation must be carried out. This is due to the fact that the Support Vector Machine (SVM) algorithms are sensitive to large differences in the scale for particular characteristics (depths) of the input data [73]. To this end, a popular standardisation method known as Z-score can be used [74]:

$$h_i^{norm} = \frac{h_i - \mu}{\sigma} \tag{8}$$

where:

h_i^{norm} —standardised value of the *i*-th depth (–),

h_i—measured value of the *i*-th depth (m),

μ—averaged depth value (m),

σ—standard deviation of the depth (m).

After preparing the training set, the standardised depth data can be used to create a mathematical model of the seafloor. The task of the SVR algorithm is to determine such a linear function that the max possible number of depth measurements could be located no further away than ε from the approximated function. The SVR method for function approximating makes use of formula (9), which is referred to in the literature as the first optimisation problem [75]:

$$\min_w f(w), f(w) \equiv \frac{1}{2} w^T w + C \sum_{i=1}^{l} \xi_\varepsilon \left(w; h_i, z_i \right) \tag{9}$$

where:

f(w)—approximated prediction function (–),

w—weight vector (–),

C—positive hyperparameter specifying the effect of the cost function on the weight vector (–),

l—number of measurements (–),

ε—hyperparameter specifying the max deviation, the distance from the approximated straight line (–),

ξ_ε—positive distance from ε for the elements of the training set located outside the assumed max deviation (–),

z_i—real, standardised value of the i-th depth (–).

ξ_ε, which is a cost function, can be determined using the following formula:

$$\xi_\varepsilon = \max\left(\left|w^T h_i - z_i\right| - \varepsilon, 0\right)^2 \tag{10}$$

The solution to the first optimisation problem is a solution recommended for training sets with a greater number of measurements than the examined features [76]. The algorithm used to solve the first optimisation problem is the TRON method [77]. This is a two-level iterative algorithm that is responsible for the determination of the weight vector value (w^k), the determination of the confidence region (Δ_k) and the formulation of the model quadratic equation:

$$q_k(s) \equiv \nabla f\left(w^k\right)^T s + \frac{1}{2} s^T \nabla^2 f\left(w^k\right)s \tag{11}$$

where:

$f(w^k + s)$-$f(w^k)$—a function which is approximated by the model quadratic equation $q_k(s)$ (–),

$\nabla f(w)$—gradient of the approximated linear function (–),

$\nabla^2 f(w)$—generalised Hessian of the approximated function (–),

s—optimisation step that specifies the direction of the search for the weight vector (–),

k—iteration number (–).

The search for an optimum step is carried out with the second iterative layer using the following condition:

$$\min_s q(s),\, for \left\|s\right\| \leq \Delta_k \tag{12}$$

The SVR algorithm was created based on [77–79].

2.3. Coastline Extraction Component

The work on this component began with a review of the existing coastline extraction methods. Before the commencement, several criteria were specified for qualifying a method for further analyses:

1   The method must only be used for the coastline extraction from a DTM or a point cloud;
2   Measurement data will be obtained only by Airborne Laser Scanning (ALS). This means the rejection of methods based on multisensory fusion, even if the fusion involves ALS;
3   Due to the rapid development of geoinformatics and computational techniques, the proposed method had to be published within the last 10 years (2011–2021).

Nine methods for extracting the coastline were selected using the above-mentioned criteria, originating from seven scientific publications from the years 2011–2021 [80–86]. Among the analysed papers, there are those that carried out very extensive method validation using many different types of the coastline and waterbodies with different geometric and optical characteristics [87], as well as those in which the method is only tested on

a single dataset [81]. Table 5 provides a cumulative list of all the discussed papers along with the main assumptions upon which the proposed method was based.

Table 5. A list of methods for validating the results of conducted coastline extraction. Own study based on [80–86].

Author and the Year of Publication	The Manner of Method Validation
Farris A.S. et al., 2022 [80]	A discussion and comparison of three methods for extracting coastline (contour, grid, and profile). A visual comparison of the differences between individual methods. A quantitative comparison of differences by interpolating the shoreline coordinates to the transverse profiles distributed along the coastline every 50 m. Mean differences in shoreline positions, RMS differences in coastline positions, and RMS differences in shoreline positions were calculated after the mean difference was removed for each combination of methods. Statistical analysis of the uncertainty in the results for the grid and profile method.
Fernández Luque I. et al., 2012 [81]	Visual and quantitative assessment of the proposed method on a single dataset. The use of the contour method [80,88] as the reference method. Statistical analysis of the uncertainty of both methods.
Hua L.W. et al., 2021 [82]	Visual assessment of the results. A comparison of the original method with the contour method while not specifying its source.
Liu H. et al., 2011 [83]	The authors propose two methods which they validate based on a single dataset. They conduct a visual analysis of the obtained coastlines and the effect of certain parameters on the received results.
Xu S., Xu S., 2018 [84]	Visual and quantitative assessment of the coastline extraction. A comparison of the extraction results on five datasets. Accuracy metrics (correctness and completeness) were calculated. The comparison was carried out in relation to the manually marked coastline courses. The results were referred to four different papers. However, only the achieved accuracies obtained on different datasets were compared.
Yousef A.H. et al., 2013a [85]	Visual assessment of the coastline extraction using a proprietary morphological algorithm. The comparison was made for two datasets. There is no comparison of the obtained results with other methods.
Yousef A.H. et al., 2013b [86]	A supplement in relation to the above paper. The same datasets and one additional set (originating from the same source) were used. A quantitative assessment of the extraction results was conducted. The accuracy assessment was carried out based on the transverse profiles determined along the manually specified coastline. The obtained results were compared with the results obtained by the method [83,89], as well as the proprietary method using the SVM classifier [85]. The method [89] and the SVM classifier made use of the data from other sensors (aerial images and an orthophotomap). Additionally, the authors carried out an estimation of errors and standard deviations using a Monte Carlo simulation of both methods proposed by them.

It was noted that the majority of the methods use information concerning the tides or base the point identification on the density and elevation indicators. Moreover, it is common practice to carry out only a visual assessment of the coastline extraction. Attention was also paid to the need for the creation of standardised reference methods in order to facilitate the performance of quantitative comparisons of the accuracy of particular methods.

Based on the conducted analyses, the parametric method was chosen [87]. An important advantage of the method is the use of only geometrical properties of the LiDAR point cloud in order to carry out the coastline extraction. Moreover, the parametric nature of the method enables the full automation of the extraction process and offers the possibility of conducting further research to attempt to develop specific parameter values for a particular measurement (coastline type, measurement conditions, and waterbody type).

The authors also compared the accuracy level that they successfully achieved using their method with four other studies on similar subjects [90–93]. Based on the conducted comparative analysis, it was concluded that the accuracy level achieved in the study concerned (1 m) was higher than that for the other reference methods (1.5–31 m). The proposed method meets the accuracy requirements provided for the most stringent IHO order, i.e., the Exclusive Order (horizontal position error ≤ 5 m (p = 0.95)) [28], which refers to papers related to the determination of the coastline course.

The method proposed by [87] is a parametric method of the coastline extraction based on the point cloud obtained by LiDAR measurements (Figure 5). It can be divided into two main parts. The first part aims to identify and cluster land returns, while the second part focuses on the coastline extraction. Both parts of the algorithm are briefly described below.
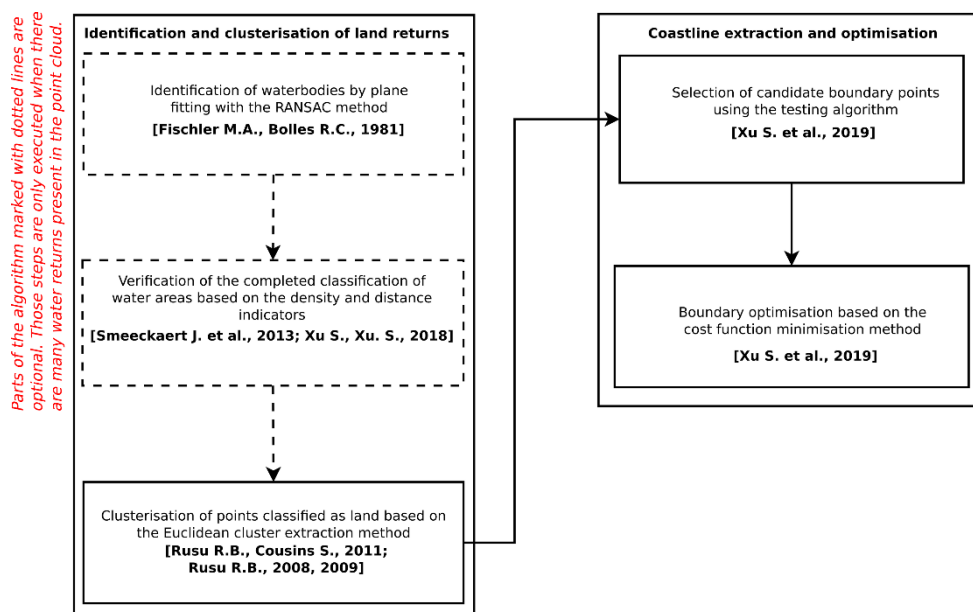

Figure 5. Diagram of the algorithm operation for coastline extraction. Own study based on [87].

The execution of the identification and clusterisation of land returns process depends on the estimated amount of returns received from waterbodies in the area. If the point cloud does not contain multiple returns from water surfaces, the Euclidean clustering algorithm [94,95] is used in order to divide points into separate clusters. However, if multiple returns from waterbodies are present or expected in the area (e.g., due to presence of marshes), the first part is extended with the detection of points belonging to the water surface. To this end, plane fitting using the RANdom SAmple Consensus (RANSAC) method [84] was used. As authors [87] have noted, the extracted plane may contain false waterbodies. To remove points mistakenly marked as water, density and elevation characteristics [96] of individual points were used. Afterwards, all the points marked as land are clustered using the aforementioned Euclidean clustering algorithm.

The second part of the algorithm involves the indication of potential boundary points and the optimisation of the boundary composed from them. The authors [87] proposed a novel method, which involves the minimum-cost path model for optimising the coastline cost function, and a testing algorithm for identifying potential boundary points from all of the candidate (land) points.

As presented in Figure 5, the algorithm for coastline extraction, proposed by [87], comprises five steps, two of which are optional and are only executed when large portion of the point cloud is associated with water returns. All of the steps presented in Figure 5 were briefly described below:

1. This step is only performed if the user marks the original LiDAR point cloud, which contains many water returns. Classification of particular clusters as water or land clusters based on the assumption of water area flatness. To this end, plane fitting by the RANSAC method is used [97]. Successive steps of the RANSAC algorithm when solving the plane fitting problem can be described as follows [95]:

   - Randomly select three non-collinear points *p* from the set of points *P*;
   - Based on the selected points, calculate the coefficients of the plane model equation;
   - Calculate the distance between the plane model and each point *p*;
   - Calculate the number of points *p* whose distance from the plane is smaller than the threshold value ϵ provided by the user.

   The RANSAC algorithm is iterative in nature. Its performance is repeated for a max of *N* times until the percentage of the points located within the tolerance limits ϵ is no greater than τ [98]. According to the authors [87], the above approach allows for identification of waterbodies larger than 500 m × 500 m.

2. This step is only performed if the user marks the original LiDAR point cloud, which contains many water returns. Verification of the completed classification of water areas based on the density and distance indicators [96] calculated for individual points. This is because the reflections from the water surface, identified based on the flatness index, can also originate from flat land areas. At this stage, two characteristics are calculated: point density (*D*), which is calculated in a rectangular window of the predefined size for every point in the cloud and the elevation of each point in the cloud above its nearest extracted plane (*E*). The above characteristics allow for reclassification of points. Points are converted to the land class if the point density D_c calculated in the predefined window is greater than the adopted threshold value T_D:

$$D_C > T_D \tag{13}$$

   Moreover, selected points are removed from the LiDAR cloud. A point is removed if its elevation above the nearest plane *E* is greater than the threshold value T_e:

$$E > T_e \tag{14}$$

3. Clusterisation of points classified as land (or all points in case the previous steps were not performed) based on the Euclidean cluster extraction method [94,95,99]. The rejection of clusters containing fewer than n_p points. It should be noted that if not too many reflections from water were noted during laser scanning, this stage already enables a significant reduction in water points in the cloud. Otherwise (e.g., in shallow waterbodies), this procedure will not ensure the removal of water points from the cloud [84], hence why authors [87] proposed the two optional steps for the case of abundant water reflections, which were described above.

4. Selection of candidate boundary points using the test algorithm [87]. During the initialisation, all points are regarded as indeterminate ones. In each step, if point *p* is an indeterminate point, it is necessary to select its *k*-nearest neighbours and, based on them, to construct a convex hull. It should be noted that in the convex hull, point *p* is not a boundary point of the convex set *S*, if it is located within a triangle whose vertices are located in *S* [100]. Hence, the points formed within the hull can be regarded as points that do not form the coastline. This process is iteratively repeated until there are no more points that can be eliminated in the above manner. Moreover, if a point is located further than T_d from the remaining points, it will be regarded as an error and immediately removed. A problem at this stage of the algorithm operation is the ambiguity of determining the coastline course based on the obtained set of points.

For example, for 5 points, it is possible to indicate many different ways to combine them, thus obtaining many different potential coastline courses (Figure 6).
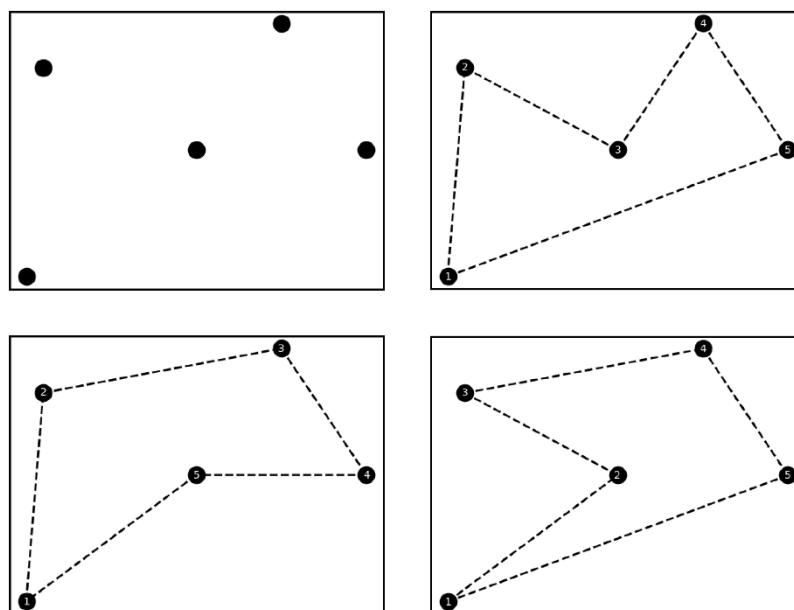

Figure 6. The ambiguity problem of determining the coastline course based on a set comprising five points. Own study based on [87].

5. Boundary optimisation based on the cost function minimisation method [87]. As there are many potential coastline courses, it is necessary to define the criterion for assessing individual connections. It is proposed that the principle of parsimony should be used [101], according to which, if a particular phenomenon or process can be explained in many ways, the one with the lowest cost (the simplest and most economical) will be the most probable. In order to assess the cost of coastline formation, the boundary cost β (m) is defined as follows:

$$\beta = \sum_{i=1}^{n}\left(D\left(B_i\right) + \sum_{\{B_i,B_j\}\in N} \lambda \left|\cos\left(\frac{\langle B_i, B_j \rangle}{2}\right)\right| \right) \tag{15}$$

where:
n—number of connections in the formed boundary (–),
$D(B_i)$—length of the connection B_i (m),
λ—weight coefficient (–),
N—number of connections in the formed boundary (–),
$<B_i,B_j>$—angle between connections B_i and B_j (°).
It should be noted that the minimisation of Equation (15) occurs when the boundary points are located close to each other, and the angles between individual connections are wide (Figure 7).
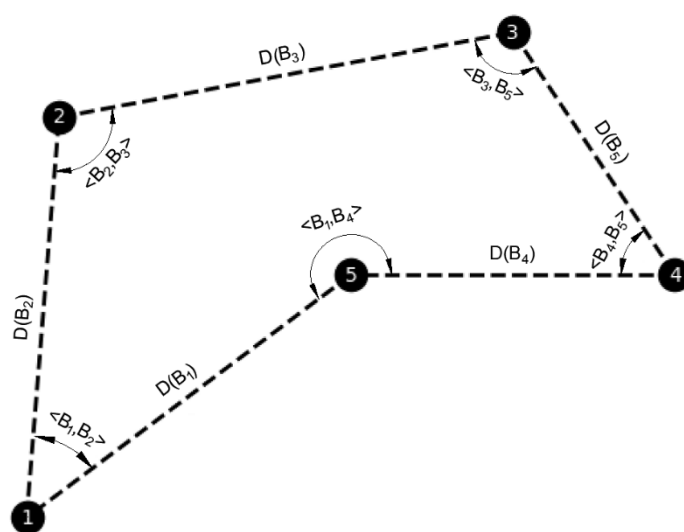
Figure 7. Visualisation of the weights calculated for individual coastline connections. Own study based on [87].

The parameter values adopted in steps 1–5 are set by the user. The authors [87] presented the values proposed by them (Table 6), noting that the method may need to be parameterised for a specific waterbody.

Table 6. The parameters of the method proposed by [87] along with the value ranges, the suggested values, and the unit.

Stage	Parameter	Range	Suggested Value	Unit
Removal of waterbodies	n_p	500–10,000	500	pt
	T_e	0.5–5	2	m
	T_D	0.1–0.5	0.3	pt/m^2
Coastline optimisation	k	20–100	50	pt
	T_d	0.5–3	2	m
	λ	1–10	3	–
	T_b	0.1–1	0.5	m

It is worth noting that the method proposed by [87] contains several underlying parameters, which were not mentioned by the authors. An example of such parameter is cluster tolerance argument used in the Euclidean clustering algorithm [94,95,99]. The implementation of the coastline extraction method [87] will allow to address this gap by careful identification of all of the parameters used in the extraction method during the software development process and their suggested ranges during the validation process. Full availability of data enables for robust verification of the correctness of the implementation process and should provide answers to the above issues. Moreover, as authors have noted, it is possible to modify the energy function (e.g., by adding curvature information to smooth the boundary in erosion regions). Therefore, the method implementation is interesting in the context of the possibility of its further enhancement and development.

3. Discussion and Conclusions

The model for the integration of data acquired by UAVs and USVs for the purposes of bathymetric monitoring shallow waterbodies (the INNOBAT system) will comprise three technology components. The first of them is the hydroacoustic and optoelectronic data integration component proposed by Dąbrowski et al. [45]. The accuracy analysis showed that the standard deviations of the differences between the coordinates modelled by Dąbrowski's method in relation to the reference coordinates amounted to easting,

northing, and height coordinates, respectively: 0.022 m, 0.040 m, and 0.019 m. A criterion for the selection of this method was the accuracy of the geospatial data harmonisation from among all the analysed methods [22,45–47]. The second criterion is the radiometric depth determination component based on optoelectronic data using the SVR method [59]. The accuracy analysis showed that the standard deviation of the depth measurement error was 0.11–0.19 m for depths ranging from 0.1 to 5.57 m. The criteria for the selection of this method included the depth measurement accuracy, hydrometeorological conditions occurring during the performance of photogrammetric surveys and the measurement equipment used from among all the analysed methods [12,57–61]. The third criterion is the coastline extraction component proposed by Xu et al. [87] An accuracy analysis showed that the standard deviation of the error in determining the shoreline position was 1 m. The criteria for the selection of this method included the automation of the extraction process and the accuracy of determining the coastline position from among all the analysed methods [80–86].

The INNOBAT system will enable, as compared to other popular bathymetric monitoring systems, such as: hydroacoustic sounding in ultra-shallow waterbodies using classical manned vehicles [29] and methods for determining waterbody depths using high-resolution satellite images [30–32], the accurate and precise measurement of the entire coastal relief based on the data acquired from UAV and USV, as well as three proposed technology components. Multisensor data fusion acquired from autonomous unmanned aerial and surface vehicles will allow to meet the requirements provided for the IHO Special Order (horizontal position error ≤ 2 m ($p = 0.95$), vertical position error ≤ 0.25 m ($p = 0.95$)).

The operational requirements of the INNOBAT system are as follows. An UAV must be equipped with a GNSS/INS system operating in the RTK mode, a LiDAR, and a photogrammetric camera. A photogrammetric flight should be made at an appropriate height (up to 100 m), so that it is smaller than the LiDAR range and the Ground Sampling Distance (GSD) does not exceed 2 cm. When it comes to the water transparency, it should be approx. 2 m. This is due to the fact that manned vessels, on which echo sounders are mounted, perform bathymetric measurements to a min. safe operational depth of approx. 2 m. As for the USV, it must be equipped with a GNSS/INS system operating in the RTK mode and a MBES. Hydrographic surveys shall be performed in windless weather and the water level is 0 in the Douglas sea scale (no waves or sea currents). However, the mission with the use of an UAV should take place in appropriate meteorological conditions, i.e., no precipitation, windless weather (wind speed not exceeding 6–7 m/s), sunny day.

Incorrect bathymetric monitoring of shallow waterbodies and those with high dynamics of hydromorphological changes can result in an adverse impact on the aquatic environment and humans. Therefore, the development of bathymetric monitoring systems seems necessary due to the fact that in recent years, there has been a very rapid improvement of measurement techniques (UAV and USV) enabling the implementation of hydrographic surveys in shallow waterbodies, as well as computational techniques for modelling the seabed relief.

Author Contributions: Conceptualisation, O.L., M.S. (Mariusz Specht), and A.S.; formal analysis, B.S. and A.H.; investigation, B.S., M.S. (Marcin Stateczny), and S.W.; methodology, O.L. and M.S. (Mariusz Specht); supervision, C.S., G.D., and D.B.; visualisation, A.H., M.S. (Marcin Stateczny), and S.W.; writing—original draft, O.L., M.S. (Mariusz Specht), and A.S.; writing—review and editing, C.S., G.D., and D.B. All authors have read and agreed to the published version of the manuscript.

Data Availability Statement: Not applicable.

References

1. Giordano, F.; Mattei, G.; Parente, C.; Peluso, F.; Santamaria, R. Integrating Sensors into a Marine Drone for Bathymetric 3D Surveys in Shallow Waters. *Sensors* **2016**, *16*, 41.
2. Giordano, F.; Mattei, G.; Parente, C.; Peluso, F.; Santamaria, R. MicroVEGA (Micro Vessel for Geodetics Application): A Marine Drone for the Acquisition of Bathymetric Data for GIS Applications. *Int. Arch. Photogramm. Remote Sens. Spat. Inf. Sci.* **2015**, *40*, 123–130.
3. Jin, J.; Zhang, J.; Shao, F.; Lyu, Z.; Wang, D. A Novel Ocean Bathymetry Technology Based on an Unmanned Surface Vehicle. *Acta Oceanol. Sin.* **2018**, *37*, 99–106.
4. Liang, J.; Zhang, J.; Ma, Y.; Zhang, C.-Y. Derivation of Bathymetry from High-resolution Optical Satellite Imagery and USV Sounding Data. *Mar. Geod.* **2017**, *40*, 466–479.
5. Lubczonek, J.; Kazimierski, W.; Zaniewicz, G.; Lacka, M. Methodology for Combining Data Acquired by Unmanned Surface and Aerial Vehicles to Create Digital Bathymetric Models in Shallow and Ultra-shallow Waters. *Remote Sens.* **2022**, *14*, 105.
6. Nikolakopoulos, K.G.; Lampropoulou, P.; Fakiris, E.; Sardelianos, D.; Papatheodorou, G. Synergistic Use of UAV and USV Data and Petrographic Analyses for the Investigation of Beachrock Formations: A Case Study from Syros Island, Aegean Sea, Greece. *Minerals* **2018**, *8*, 534.
7. Specht, M.; Specht, C.; Stateczny, A.; Marchel, Ł.; Lewicka, O.; Paliszewska-Mojsiuk, M.; Wiśniewska, M. Determining the Seasonal Variability of the Territorial Sea Baseline in Poland (2018–2020) Using Integrated USV/GNSS/SBES Measurements. *Energies* **2021**, *14*, 2693.
8. Specht, M.; Specht, C.; Szafran, M.; Makar, A.; Dąbrowski, P.; Lasota, H.; Cywiński, P. The Use of USV to Develop Navigational and Bathymetric Charts of Yacht Ports on the Example of National Sailing Centre in Gdańsk. *Remote Sens.* **2020**, *12*, 2585.
9. Stateczny, A.; Grońska, D.; Motyl, W. Hydrodron—New Step for Professional Hydrography for Restricted Waters. In Proceedings of the Baltic Geodetic Congress 2018 (BGC 2018), Olsztyn, Poland, 21–23 June 2018.
10. Suhari, K.T.; Karim, H.; Gunawan, P.H.; Purwanto, H. Small ROV Marine Boat for Bathymetry Surveys of Shallow Waters—Potential Implementation in Malaysia. *Int. Arch. Photogramm. Remote Sens. Spat. Inf. Sci.-ISPRS Arch.* **2017**, *XLII-4/W5*, 201–208.
11. Alevizos, E.; Oikonomou, D.; Argyriou, A.V.; Alexakis, D.D. Fusion of Drone-based RGB and Multi-spectral Imagery for Shallow Water Bathymetry Inversion. *Remote Sens.* **2022**, *14*, 1127.
12. Bagheri, O.; Ghodsian, M.; Saadatseresht, M. Reach Scale Application of UAV+SfM Method in Shallow Rivers Hyperspatial Bathymetry. *Int. Arch. Photogramm. Remote Sens. Spat. Inf. Sci.* **2015**, *XL-1/W5*, 77–81.
13. Bandini, F.; Lopez-Tamayo, A.; Merediz-Alonso, G.; Olesen, D.; Jakobsen, J.; Wang, S.; Garcia, M.; Bauer-Gottwein, P. Unmanned Aerial Vehicle Observations of Water Surface Elevation and Bathymetry in the Cenotes and Lagoons of the Yucatan Peninsula, Mexico. *Hydrogeol. J.* **2018**, *26*, 2213–2228.
14. Bandini, F.; Olesen, D.; Jakobsen, J.; Kittel, C.M.M.; Wang, S.; Garcia, M.; Bauer-Gottwein, P. Technical Note: Bathymetry Observations of Inland Water Bodies Using a Tethered Single-beam Sonar Controlled by an Unmanned Aerial Vehicle. *Hydrol. Earth Syst. Sci.* **2018**, *22*, 4165–4181.
15. He, J.; Lin, J.; Ma, M.; Liao, X. Mapping Topo-bathymetry of Transparent Tufa Lakes Using UAV-based Photogrammetry and RGB Imagery. *Geomorphology* **2021**, *389*, 107832.
16. Kim, J.S.; Baek, D.; Seo, I.W.; Shin, J. Retrieving Shallow Stream Bathymetry from UAV-assisted RGB Imagery Using a Geospatial Regression Method. *Geomorphology* **2019**, *341*, 102–114.
17. Massuel, S.; Feurer, D.; El Maaoui, M.A.; Calvez, R. Deriving Bathymetries from Unmanned Aerial Vehicles: A Case Study of a Small Intermittent Reservoir. *Hydrol. Sci. J.* **2022**, *67*, 82–93.
18. Panlilio, K.; Pedido, S.M.; Ramos, R.; Tamondong, A. Bathymetric Mapping of Shallow Waters in Lian, Batangas Using Unmanned Aerial Vehicle (UAV). In Proceedings of the 40th Asian Conference on Remote Sensing (ACRS 2019), Daejeon, Korea, 14–18 October 2019.
19. Cao, B.; Fang, Y.; Jiang, Z.; Gao, L.; Hu, H. Shallow Water Bathymetry from WorldView-2 Stereo Imagery Using Two-media Photogrammetry. *Eur. J. Remote Sens.* **2019**, *52*, 506–521.
20. Popielarczyk, D.; Marschalko, M.; Templin, T.; Niemiec, D.; Yilmaz, I.; Matuszková, B. Bathymetric Monitoring of Alluvial River Bottom Changes for Purposes of Stability of Water Power Plant Structure with a New Methodology for River Bottom Hazard Mapping (Wloclawek, Poland). *Sensors* **2020**, *20*, 5004.
21. Khazaei, B.; Read, L.K.; Casali, M.; Sampson, K.M.; Yates, D.N. GLOBathy, the Global Lakes Bathymetry Dataset. *Sci. Data* **2022**, *9*, 36.
22. Erena, M.; Atenza, J.F.; García-Galiano, S.; Domínguez, J.A.; Bernabé, J.M. Use of Drones for the Topo-bathymetric Monitoring of the Reservoirs of the Segura River Basin. *Water* **2019**, *11*, 445.
23. Pratomo, D.G.; Khomsin; Putranto, B.F.E. Analysis of the Green Light Penetration from Airborne LiDAR Bathymetry in Shallow Water Area. In *IOP Conference Series: Earth and Environmental Science*; IOP Publishing: Bristol, UK, 2019; Volume 389, pp. 012003.
24. Wang, D.; Xing, S.; He, Y.; Yu, J.; Xu, Q.; Li, P. Evaluation of a New Lightweight UAV-borne Topo-bathymetric LiDAR for Shallow Water Bathymetry and Object Detection. *Sensors* **2022**, *22*, 1379.
25. Hattori, N.; Sato, S.; Yamanaka, Y. Development of an Imagery-based Monitoring System for Nearshore Bathymetry by Using Wave Breaking Density. *Coast. Eng.* **2019**, *61*, 308–320.

26. Salameh, E.; Frappart, F.; Almar, R.; Baptista, P.; Heygster, G.; Lubac, B.; Raucoules, D.; Almeida, L.P.; Bergsma, E.W.J.; Capo, S.; et al. Monitoring Beach Topography and Nearshore Bathymetry Using Spaceborne Remote Sensing: A Review. *Remote Sens.* **2019**, *11*, 2212.

27. Specht, M.; Stateczny, A.; Specht, C.; Widźgowski, S.; Lewicka, O.; Wiśniewska, M. Concept of an Innovative Autonomous Unmanned System for Bathymetric Monitoring of Shallow Waterbodies (INNOBAT System). *Energies* **2021**, *14*, 5370.

28. IHO. *IHO Standards for Hydrographic Surveys*, 6th ed.; Special Publication No. 44; IHO: Monaco, Monaco, 2020.

29. Specht, C.; Lewicka, O.; Specht, M.; Dąbrowski, P.; Burdziakowski, P. Methodology for Carrying out Measurements of the Tombolo Geomorphic Landform Using Unmanned Aerial and Surface Vehicles near Sopot Pier, Poland. *J. Mar. Sci. Eng.* **2020**, *8*, 384.

30. Hogrefe, K.R.; Wright, D.J.; Hochberg, E.J. Derivation and Integration of Shallow-water Bathymetry: Implications for Coastal Terrain Modeling and Subsequent Analyses. *Mar. Geod.* **2008**, *31*, 299–317.

31. Kulawiak, M.; Chybicki, A. Application of Web-GIS and Geovisual Analytics to Monitoring of Seabed Evolution in South Baltic Sea Coastal Areas. *Mar. Geod.* **2018**, *41*, 405–426.

32. Warnasuriya, T.W.S.; Gunaalan, K.; Gunasekara, S.S. Google Earth: A New Resource for Shoreline Change Estimation—Case Study from Jaffna Peninsula, Sri Lanka. *Mar. Geod.* **2018**, *41*, 546–580.

33. Lihua, Z.; Shuaidong, J.; Rencan, P.; Jian, D.; Ning, L. A Quantitative Method to Control and Adjust the Accuracy of Adaptive Grid Depth Modeling. *Mar. Geod.* **2013**, *36*, 408–427.

34. Makar, A. The Sea Bottom Surface Described by Coons Pieces. *Sci. J. Marit. Univ. Szczec.* **2016**, *45*, 187–190.

35. Sassais, R.; Makar, A. Methods to Generate Numerical Models of Terrain for Spatial ENC Presentation. *Annu. Navig.* **2011**, *18*, 1–13.

36. Aurelia Technologies Inc. Aurelia X8 Standard. Available online: https://aurelia-aerospace.com/product/aurelia-x8-standard/ (accessed on 19 August 2022).

37. SBG Systems. Ellipse-D. Available online: https://www.sbg-systems.com/products/ellipse-series/#ellipse_d_rtk_gnss_ins (accessed on 19 August 2022).

38. SBG Systems. Ekinox Series. Available online: https://www.sbg-systems.com/products/ekinox-series/ (accessed on 19 August 2022).

39. Velodyne Lidar. Puck LITE. Available online: https://velodynelidar.com/products/puck-lite/ (accessed on 19 August 2022).

40. Sony Corporation. α6500 Premium E-mount APS-C Camera. Available online: https://www.sony.com/en-ae/electronics/interchangeable-lens-cameras/ilce-6500-body-kit (accessed on 19 August 2022).

41. Sony Corporation. E 35mm F1.8 OSS. Available online: https://www.sony.com/en-ae/electronics/camera-lenses/sel35f18 (accessed on 19 August 2022).

42. Gremsy. GREMSY T3V3. Available online: https://gremsy.com/gremsy-t3v3-store (accessed on 19 August 2022).

43. Burdziakowski, P.; Stateczny, A. Universal Autonomous Control and Management System for Multipurpose Unmanned Surface Vessel. *Pol. Marit. Res.* **2019**, *26*, 30–39.

44. Ping DSP Inc. 3DSS-DX-450. Available online: https://www.pingdsp.com/3DSS-DX-450 (accessed on 19 August 2022).

45. Dąbrowski, P.S.; Specht, C.; Specht, M.; Burdziakowski, P.; Makar, A.; Lewicka, O. Integration of Multi-source Geospatial Data from GNSS Receivers, Terrestrial Laser Scanners, and Unmanned Aerial Vehicles. *Can. J. Remote Sens.* **2021**, *47*, 621–634.

46. Genchi, S.A.; Vitale, A.J.; Perillo, G.M.E.; Seitz, C.; Delrieux, C.A. Mapping Topobathymetry in a Shallow Tidal Environment Using Low-cost Technology. *Remote Sens.* **2020**, *12*, 1394.

47. Gesch, D.; Wilson, R. Development of a Seamless Multisource Topographic/Bathymetric Elevation Model of Tampa Bay. *Mar. Technol. Soc. J.* **2001**, *35*, 58–64.

48. Lewicka, O.; Specht, M.; Stateczny, A.; Specht, C.; Brčić, D.; Jugović, A.; Widźgowski, S.; Wiśniewska, M. Analysis of GNSS, Hydroacoustic and Optoelectronic Data Integration Methods Used in Hydrography. *Sensors* **2021**, *21*, 7831.

49. Burdziakowski, P.; Specht, C.; Dabrowski, P.S.; Specht, M.; Lewicka, O.; Makar, A. Using UAV Photogrammetry to Analyse Changes in the Coastal Zone Based on the Sopot Tombolo (Salient) Measurement Project. *Sensors* **2020**, *20*, 4000.

50. Grafarend, E. The Optimal Universal Transverse Mercator Projection. In *Geodetic Theory Today*; Sansò, F., Ed.; Springer: Berlin/Heidelberg, Germany, 1995; Volume 114, pp. 51.

51. Council of Ministers of the Republic of Poland. *Ordinance of the Council of Ministers of 15 October 2012 on the National Spatial Reference System*; Council of Ministers of the Republic of Poland: Warsaw, Poland, 2012. (In Polish).

52. Ministry of National Defence of the Republic of Poland. *Ordinance of the Minister of National Defense of 28 March 2018 on Minimum Requirements for Hydrographic Surveys*; Ministry of National Defence of the Republic of Poland: Warsaw, Poland, 2018. (In Polish)

53. Council of Ministers of the Republic of Poland. *Ordinance of the Council of Ministers of 19 December 2019 Amending the Ordinance Regarding National Spatial Reference System*; Council of Ministers of the Republic of Poland: Warsaw, Poland, 2019. (In Polish)

54. Specht, M.; Specht, C.; Wąż, M.; Naus, K.; Grządziel, A.; Iwen, D. Methodology for Performing Territorial Sea Baseline Measurements in Selected Waterbodies of Poland. *Appl. Sci.* **2019**, *9*, 3053.

55. UKHO. *ADMIRALTY Tide Tables*; UKHO: Taunton, UK, 2019.

56. Lewicka, O.; Specht, M.; Stateczny, A.; Specht, C.; Dyrcz, C.; Dąbrowski, P.; Szostak, B.; Halicki, A.; Stateczny, M.; Widźgowski, S. Analysis of Transformation Methods of Hydroacoustic and Optoelectronic Data Based on the Tombolo Measurement Campaign in Sopot. *Remote Sens.* **2022**, *14*, 3525.

57. Holman, R.; Plant, N.; Holland, T. cBathy: A Robust Algorithm for Estimating Nearshore Bathymetry. *J. Geophys. Res. Oceans* **2013**, *118*, 2595–2609.

58. Hashimoto, K.; Shimozono, T.; Matsuba, Y.; Okabe, T. Unmanned Aerial Vehicle Depth Inversion to Monitor River-mouth Bar Dynamics. *Remote Sens.* **2021**, *13*, 412.

59. Agrafiotis, P.; Skarlatos, D.; Georgopoulos, A.; Karantzalos, K. Shallow Water Bathymetry Mapping from UAV Imagery Based on Machine Learning. *Int. Arch. Photogramm. Remote Sens. Spat. Inf. Sci.* **2019**, *XLII-2/W10*, 9–16.

60. Simarro, G.; Calvete, D.; Luque, P.; Orfila, A.; Ribas, F. UBathy: A New Approach for Bathymetric Inversion from Video Imagery. *Remote Sens.* **2019**, *11*, 2722.

61. Tonion, F.; Pirotti, F.; Faina, G.; Paltrinieri, D. A Machine Learning Approach to Multispectral Satellite Derived Bathymetry. *ISPRS Ann. Photogramm. Remote Sens. Spatial Inf. Sci.* **2020**, *V-3-2020*, 565–570.

62. da Silva Santos, C.E.; Sampaio, R.C.; Coelho, L.D.S.; Bestard, G.A.; Llanos, C.H. Multi-objective Adaptive Differential Evolution for SVM/SVR Hyperparameters Selection. *Pattern Recognit.* **2021**, *110*, 107649.

63. Basak, D.; Pal, S.; Patranabis, D.C. Support Vector Regression. *Neural Inf. Process.–Lett. Rev.* **2007**, *11*, 203–224.

64. Cao, B.; Deng, R.; Zhu, S. Universal Algorithm for Water Depth Refraction Correction in Through-water Stereo Remote Sensing. *Int. J. Appl. Earth Obs. Geoinf.* **2020**, *91*, 102108.

65. Condorelli, F.; Rinaudo, F.; Salvadore, F.; Tagliaventi, S. A Match-moving Method Combining AI and SFM Algorithms in Historical Film Footage. *Int. Arch. Photogramm. Remote Sens. Spatial Inf. Sci.* **2020**, *XLIII-B2-2020*, 813–820.

66. Chandrashekar, A.; Papadakis, J.; Willis, A.; Gantert, J. Structure-from-Motion and RGBD Depth Fusion. In Proceedings of the IEEE Southeastcon 2018, St. Petersburg, FL, USA, 19–22 April 2018.

67. Eltner, A.; Sofia, G. Chapter 1-Structure from Motion Photogrammetric Technique. In *Developments in Earth Surface Processes*; Elsevier: Amsterdam, The Netherlands, 2020; Volume 23, pp. 1–24.

68. Anders, N.; Valente, J.; Masselink, R.; Keesstra, S. Comparing Filtering Techniques for Removing Vegetation from UAV-based Photogrammetric Point Clouds. *Drones* **2019**, *3*, 61.

69. Serifoglu Yilmaz, C.; Gungor, O. Comparison of the Performances of Ground Filtering Algorithms and DTM Generation from a UAV-based Point Cloud. *Geocarto Int.* **2018**, *33*, 522–537.

70. Wallace, L.; Lucieer, A.; Malenovský, Z.; Turner, D.; Vopěnka, P. Assessment of Forest Structure Using Two UAV Techniques: A Comparison of Airborne Laser Scanning and Structure from Motion (SfM) Point Clouds. *Forests* **2016**, *7*, 62.

71. Nadal-Romero, E.; Revuelto, J.; Errea, P.; López-Moreno, J. The Application of Terrestrial Laser Scanner and SfM Photogrammetry in Measuring Erosion and Deposition Processes in Two Opposite Slopes in a Humid Badlands Area (Central Spanish Pyrenees). *SOIL* **2015**, *1*, 561–573.

72. Kraus, K.; Pfeifer, N. Determination of Terrain Models in Wooded Areas with Airborne Laser Scanner Data. *ISPRS J. Photogramm. Remote Sens.* **1998**, *53*, 193–203.

73. Géron, A. *Hands-On Machine Learning with Scikit-Learn, Keras, and TensorFlow: Concepts, Tools, and Techniques to Build Intelligent Systems*, 2nd ed.; O'Reilly Media, Inc.: Newton, MA, USA, 2019.

74. Patro, S.; Sahu, K.K. Normalization: A Preprocessing Stage. *IARJSET* **2015**, *2*, 20–22.

75. Smola, A.J.; Schölkopf, B. A Tutorial on Support Vector Regression. *Stat. Comput.* **2004**, *14*, 199–222.

76. Pedregosa, F.; Varoquaux, G.; Gramfort, A.; Michel, V.; Thirion, B.; Grisel, O.; Blondel, M.; Prettenhofer, P.; Weiss, R.; Dubourg, V.; et al. Scikit-learn: Machine Learning in Python. *J. Mach. Learn. Res.* **2011**, *12*, 2825–2830.

77. Chia-Hua, H.; Chih-Jen, L. Large-scale Linear Support Vector Regression. *J. Mach. Learn. Res.* **2012**, *13*, 3323–3348.

78. Lin, C.-J.; Moré, J.J. Newton's Method for Large Bound-constrained Optimization Problems. *SIAM J. Optim.* **1999**, *9*, 1100–1127.

79. Lin, C.-J.; Weng, R.C.; Keerthi, S.S. Trust Region Newton Method for Large-scale Logistic Regression. *J. Mach. Learn. Res.* **2008**, *9*, 627–650.

80. Farris, A.S.; Weber, K.M.; Doran, K.S.; List, J.H. Comparing Methods Used by the U.S. Geological Survey Coastal and Marine Geology Program for Deriving Shoreline Position from Lidar Data. Available online: https://pubs.usgs.gov/of/2018/1121/ofr20181121.pdf (accessed on 19 August 2022).

81. Fernández Luque, I.; Aguilar Torres, F.J.; Aguilar Torres, M.A.; Pérez García, J.L.; López Arenas, A. A New, Robust, and Accurate Method to Extract Tide-coordinated Shorelines from Coastal Elevation Models. *J. Coast. Res.* **2012**, *28*, 683–699.

82. Hua, L.W.; Bi, Y.L.; Hao, L. The Research of Artificial Shoreline Extraction Based on Airborne LIDAR Data. *J. Phys. Conf. Ser.* **2021**, *2006*, 012048.

83. Liu, H.; Wang, L.; Sherman, D.J.; Wu, Q.; Su, H. Algorithmic Foundation and Software Tools for Extracting Shoreline Features from Remote Sensing Imagery and LiDAR Data. *J. Geogr. Inf. Syst.* **2011**, *3*, 99–119.

84. Xu, S.; Xu, S. A Minimum-cost Path Model to the Bridge Extraction from Airborne LiDAR Point Clouds. *J. Indian Soc. Remote Sens.* **2018**, *46*, 1423–1431.

85. Yousef, A.H.; Iftekharuddin, K.; Karim, M. A New Morphology Algorithm for Shoreline Extraction from DEM Data. In Proceedings of the SPIE Defense, Security, and Sensing 2013, Baltimore, MA, USA, 29–30 April 2013.

86. Yousef, A.H.; Iftekharuddin, K.M.; Karim, M.A. Shoreline Extraction from Light Detection and Ranging Digital Elevation Model Data and Aerial Images. *Opt. Eng.* **2013**, *53*, 011006.

87. Xu, S.; Ye, N.; Xu, S. A New Method for Shoreline Extraction from Airborne LiDAR Point Clouds. *Remote Sens. Lett.* **2019**, *10*, 496–505.

88. Stockdonf, H.F.; Sallenger Jr.; A.H.; List, J.H.; Holman, R.A. Estimation of Shoreline Position and Change Using Airborne Topographic Lidar Data. *J. Coast. Res.* **2002**, *18*, 502–513.

89. Lee, I.-C.; Wu, B.; Li, R. Shoreline Extraction from the Integration of LiDAR Point Cloud Data and Aerial Orthophotos Using Mean Shift Segmentation. In Proceedings of the American Society for Photogrammetry and Remote Sensing Annual Conference 2009 (ASPRS 2009), Baltimore, MD, USA, 9–13 March 2009.

90. Di, K.; Wang, J.; Ma, R.; Li, R. Automatic Shoreline Extraction from High-resolution IKONOS Satellite Imagery. In Proceedings of the American Society for Photogrammetry and Remote Sensing Annual Conference 2003 (ASPRS 2003), Anchorage, AK, USA, 5–9 May 2003.

91. Lee, I.-C.; Cheng, L.; Li, R. Optimal Parameter Determination for Mean-shift Segmentation-based Shoreline Extraction Using Lidar Data, Aerial Orthophotos, and Satellite Imagery. In Proceedings of the American Society for Photogrammetry and Remote Sensing Annual Conference 2010 (ASPRS 2010), San Diego, CA, USA, 26–30 April 2010.

92. Liu, H.; Sherman, D.; Gu, S. Automated Extraction of Shorelines from Airborne Light Detection and Ranging Data and Accuracy Assessment Based on Monte Carlo Simulation. *J. Coast. Res.* **2007**, *236*, 1359–1369.

93. Niedermeier, A.; Romaneeßen, E.; Lehner, S. Detection of Coastlines in SAR Images Using Wavelet Methods. *IEEE Trans. Geosci. Remote Sens.* **2000**, *38*, 2270–2281.

94. Rusu, R.B. Semantic 3d Object Maps for Everyday Manipulation in Human Living Environments. *KI-Künstliche Intell.* **2010**, *24*, 345–348.

95. Rusu, R.B. Semantic 3d Object Maps for Everyday Manipulation in Human Living Environments. Ph.D. Thesis, Technische Universität München, München, Germany, 2009.

96. Smeeckaert, J.; Mallet, C.; David, N.; Chehata, N.; Ferraz, A. Large-scale Classification of Water Areas Using Airborne Topographic LiDAR Data. *Remote Sens. Environ.* **2013**, *138*, 134–148.

97. Fischler, M.A.; Bolles, R.C. Random Sample Consensus: A Paradigm for Model Fitting with Applications to Image Analysis and Automated Cartography. *Commun. ACM* **1981**, *24*, 381–395.

98. Derpanis, K.G. Overview of the RANSAC Algorithm. Available online: http://www.cse.yorku.ca/~kosta/CompVis_Notes/ransac.pdf (accessed on 19 August 2022).

99. Rusu, R.B. Cousins, C. 3D Is Here: Point Cloud Library (PCL). In Proceedings of the IEEE International Conference on Robotics and Automation 2011 (ICRA 2011), Shanghai, China, 9–13 May 2011.

100. Wang, J.; Shan, J. Segmentation of LiDAR Point Clouds for Building Extraction. In Proceedings of the American Society for Photogrammetry and Remote Sensing Annual Conference 2009 (ASPRS 2009), Baltimore, MD, USA, 9–13 March 2009.

101. Jefferys, W.H.; Berger, J.O. Ockham's Razor and Bayesian Analysis. *Am. Sci.* **1992**, *80*, 64–72.